UCRL-JC-133047
Preprint

Room Temperature $CaGa_2S_4:Dy^{3+}$ Laser Action at 2.43 and 4.31 μm and $KPb_2Cl_5:Dy^{3+}$ Laser Action at 2.43 μm

M. C. Nostrand, R. H. Page, S. A. Payne,W. F. Krupke,
P. G. Schunemann and L. I. Isaenko

This paper was prepared for submittal to
Fourteenth Topical Meeting on Advanced Solid-State Lasers
Boston, MA
Jan. 31-Feb.3, 1999

January 28, 1999

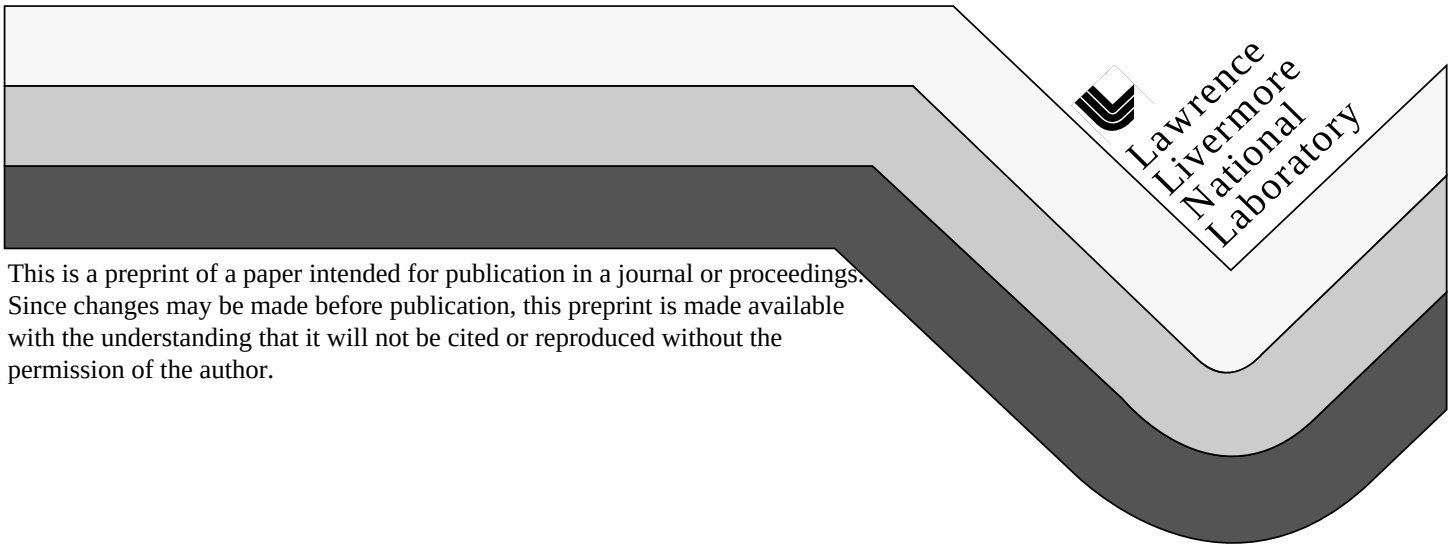

Room temperature $CaGa_2S_4:Dy^{3+}$ laser action at 2.43 and 4.31 μm and $KPb_2Cl_5:Dy^{3+}$ laser action at 2.43 μm

M.C. Nostrand, R.H. Page, S.A. Payne, and W.F. Krupke
University of California, Lawrence Livermore National Laboratory
L-482, Livermore, CA 94550
nostrand1@llnl.gov

P.G. Schunemann
Sanders, A Lockheed Martin Company
P.O. Box 868, Nashua, NH 03061-0868

L.I. Isaenko
Design and Technical Institute of Monocrystals
SB RAS, Novosibirsk, 630058 Russia

Abstract: In a previous report[1] we discussed the potential for two non-hygroscopic solid-state crystals as new hosts for Dy^{3+} lasers in the mid-IR (2-10μm) at room temperature. In this paper, we report such laser action at 2.43 and 4.31 μm in $CaGa_2S_4:Dy^{3+}$, and at 2.43 μm in $KPb_2Cl_5:Dy^{3+}$. Slope efficiencies of 2.7% and 1.6%, respectively, were achieved for the sulfide crystal and 2.2% for the chloride crystal. Findlay-Clay analysis obtained losses of 3.9%, 0.9% and 1.2%, respectively.

OCIS codes: (140.3380) Laser materials; (140.3580) Lasers, solid-state; (140.5680) Rare-earth and transition metal solid-state lasers

Introduction

Applications such as remote sensing and countermeasures have driven the need for mid-IR laser sources. This in turn has inspired the search for new low-phonon energy hosts since mid-IR luminescence in traditional oxide and fluoride hosts is quenched by non-radiative multiphonon relaxation. Sulfide[2] and chloride based hosts have been studied in this pursuit since they are the denser counterparts to oxide and fluoride hosts, thereby possessing a naturally lower maximum phonon frequency. The problem with these materials is that they typically have poor mechanical properties and are difficult to fabricate. Indeed, until now, no moisture-resistant chloride laser host has been identified. Here we demonstrate room temperature mid-IR laser action at 2.43 μm ($^6H_{9/2},^6F_{11/2} \rightarrow {}^6H_{13/2}$) and 4.31 μm ($^6H_{11/2} \rightarrow {}^6H_{13/2}$) in $CaGa_2S_4:Dy^{3+}$ and at 2.43 μm in $KPb_2Cl_5:Dy^{3+}$. Both of these hosts are *not moisture sensitive*. To our knowledge, this is the first report of laser operation on the $^6H_{9/2},^6F_{11/2} \rightarrow {}^6H_{13/2}$ transition of Dy^{3+}, of laser action beyond 4 μm in any rare-earth-doped sulfide, and of laser action in any rare-earth-doped moisture-resistant chloride.

$CaGa_2S_4$ physical properties/crystal growth

$CaGa_2S_4$ is biaxial and belongs to the orthorhombic crystal class[3]. The 1.5 cm sample used in our experiments was grown at Sanders by the horizontal gradient freeze technique in a two-zone transparent furnace. Dy^{3+} was doped on the Ca^{2+} site[4] to an estimated concentration of 8 x 10^{19} cm^{-3} (2.0 mol% in

the melt and an estimated 60% distribution coefficient). Na^+ was also added at the same level to maintain charge balance. Two axes of the biaxial indicatrix were identified at extinction positions in a polariscope. These directions are labeled 'slow' and 'fast' in Figure 2.

$CaGa_2S_4:Dy^{3+}$ spectroscopy

In our previous work,[1] spectroscopic data such as absorption cross sections, emission cross sections (σ_{em}), and lifetimes (τ_{upper}) were measured for a sample of $CaGa_2S_4:Dy^{3+}$. This data was used to perform a Judd-Ofelt analysis, yielding spectroscopic data such as radiative lifetimes (τ_{rad}), branching ratios (β), and radiative quantum yields ($\eta = \tau_{upper}/\tau_{rad}$). Table 1 gives a summary of the relevant data for the present laser sample. The Dy^{3+} energy level diagram indicating the relevant pump and laser transitions is shown in Figure 1. Figure 2 shows the absorption spectrum, polarized along the 'slow' and 'fast' axes described above. Notice the absorption at 1319 nm (the laser pump wavelength) is almost 5 times greater along the 'fast' axis.

Table 1. Spectroscopic data for $CaGa_2S_4:Dy^{3+}$.

Transition	λ (μm)	τ_{upper} (ms)	τ_{rad} (ms)	η (%)	β (%)	σ_{em} (10^{-20} cm^2)
$^6H_{9/2}$-$^6F_{11/2}$ → $^6H_{13/2}$	2.4	0.20	0.52	38	9	1.2
$^6H_{11/2}$ → $^6H_{13/2}$	4.3	3.02	4.16	73	7	0.7

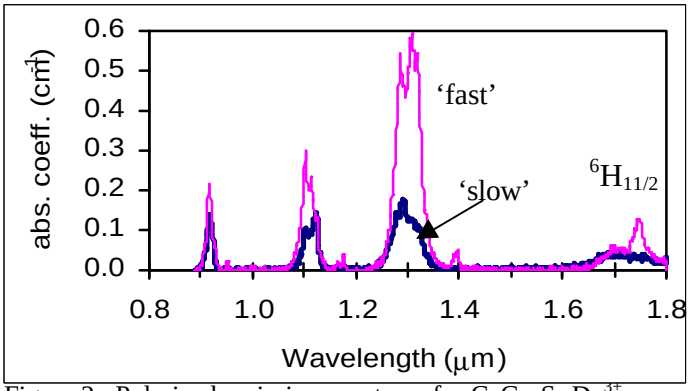

Figure 2. Polarized emission spectrum for $CaGa_2S_4:Dy^{3+}$.

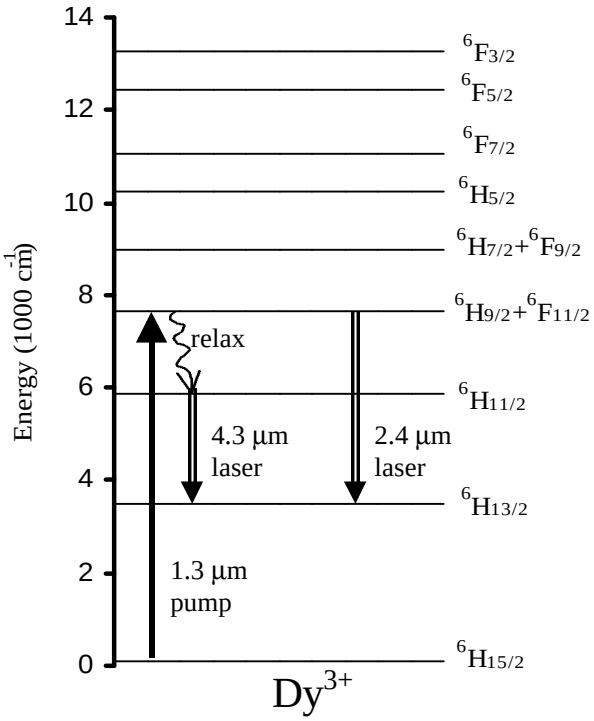

Figure 1. Energy levels and laser schemes of trivalent dysprosium.

$CaGa_2S_4:Dy^{3+}$ Experimental setup

Figure 3 shows the experimental setup for demonstrating laser action at both 2.43 and 4.31 μm. The uncoated rectangular parallelepiped sample was placed in the center of a 20 cm confocal cavity and end-pumped at normal incidence by a Nd:YAG laser operating at 1319 nm (and 1338 nm) with 75 μs, 1 Hz pulses. To avoid walk-off along the two polarization axes of the sample, the input beam was polarized along the 'fast' axis with a calcite polarizer. The pump spot profile was measured by a razor scan and fit to a Gaussian ($1/e^2$) spot size of 350 +/-10 μm. A 1500 nm long-pass filter and 10 cm CaF_2 lens focussed

the IR laser light to a 77K InSb detector for temporal waveform acquisition, or to a Molectron J3-09 pyroelectric detector for slope-efficiency measurements. A glass slide pick-off and Molectron J-25 detector measured the input pump energy. The laser output spectra were recorded with a 1-meter, 300 groove/mm grating monochromator located a few meters from the cavity. A calcite polarizer measured the polarization state of the mid-IR output.

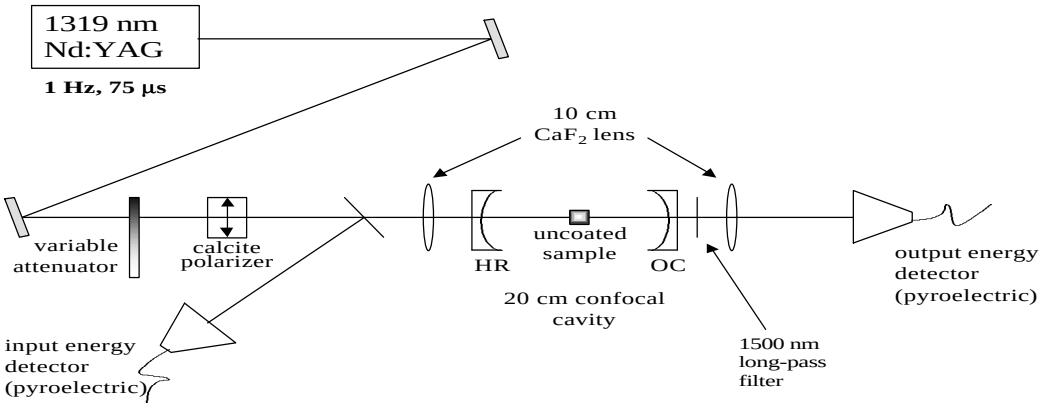

Figure 3. Experimental laser setup.

Although the sample had a 'laser-grade' polish, its end faces were not perfectly parallel. A wedge angle of ~ 3 mrad was determined by examination of reflections of a single He-Ne laser beam from both end faces of the sample.

$CaGa_2S_4:Dy^{3+}$ 2.43 μm laser results

Four cavity mirrors were available for 2.4 μm operation with transmissions of 0.36%, 0.58%, 1.65%, and 7.70%. Data was recorded for four mirror configurations with total transmissions (high reflector + output coupler) of 0.94%, 2.23%, 8.28%, and 9.35%, where each configuration obeyed $T_{HR} < T_{OC}$. Slope efficiency curves are shown in Figure 4 for two of these configurations, and all data are summarized in Table 2. Absorbed energy was limited by concerns of damage to the sample. A damage threshold was estimated to be near 15 J/cm^2 of absorbed energy. Absorbed energy is calculated from incident energy via the relation[5]

$$E_{abs} = E_{inc}\,(1-R_F)(1-e^{-\alpha l})(1-R_F e^{-\alpha l})^{-1} \qquad (1)$$

where E_{inc} is the laser energy incident on the sample, R_F is the Fresnel reflectivity, α is the absorption coefficient at the pump wavelength, and l is the sample length. Threshold estimates were made using a well-known formula for end-pumped lasers[6]

$$E_{abs}^{th} = \pi\frac{(w_p^2 + w_l^2)}{4\sigma_{em}\eta_s}\frac{hc}{\lambda_p}(L+T) \qquad (2)$$

where w_p is the minimum pump beam radius in the sample, w_l is the laser waist calculated based on cavity parameters, σ_{em} is the emission cross section, η_s is the storage efficiency of the upper laser level, L is the round-trip passive loss in the cavity, T is the total transmission (HR + OC), and λ_p is the pump wavelength. Slope efficiency was estimated using the formula[7]

$$\eta_{slope} = \eta_s \, \eta_B \, \frac{\lambda_p}{\lambda_l} \frac{T}{(L+T)} \qquad (3)$$

where η_B is the pump and laser beam overlap efficiency, calculated assuming Gaussian beam profiles, and λ_l is the laser wavelength. Predictions agreed relatively well with the measured thresholds, but were an order of magnitude higher than the measured slope efficiencies. Table 2 includes the predicted result values. The explanation for this discrepancy is not yet understood. A Findlay-Clay plot of absorbed energy threshold vs. transmission is shown in Figure 5, yielding a round-trip passive loss of L = 3.9% +/- 1.4%. Comparing this deduced loss-level to the Fresnel losses (calculated to be ~ 14% per face), we see that the Fresnel reflections may introduce uncompensated losses into the cavity due to the wedge of the sample. The laser output spectrum is shown in Figure 6, along with the unpolarized emission spectrum, showing that laser action occurs at the fluorescence peak. The laser light was determined to be polarized along the 'fast' axis.

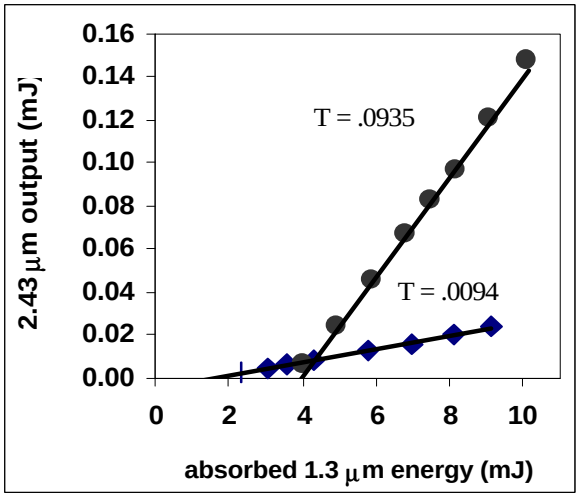

Figure 4. Slope efficiency curves for $CaGa_2S_4:Dy^{3+}$ at 2.43 μm.

Table 2. Summary of $CaGa_2S_4:Dy^{3+}$ 2.43 μm laser results.

Total output coupling (%)	Measured threshold (mJ)	Predicted threshold (mJ)	Measured slope efficiency (%)	Predicted slope efficiency (%)
0.9	1.3	1.6	0.3	5.8
2.2	2.0	2.0	1.8	10.8
8.3	3.6	4.1	2.7	20.3
9.4	4.0	4.4	2.4	21.0

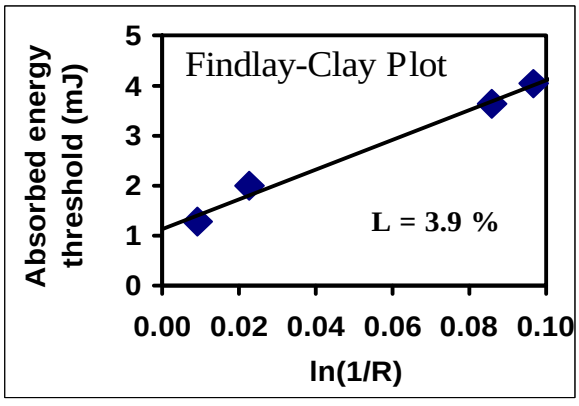

Figure 5. Plot of absorbed energy threshold vs. total transmission.

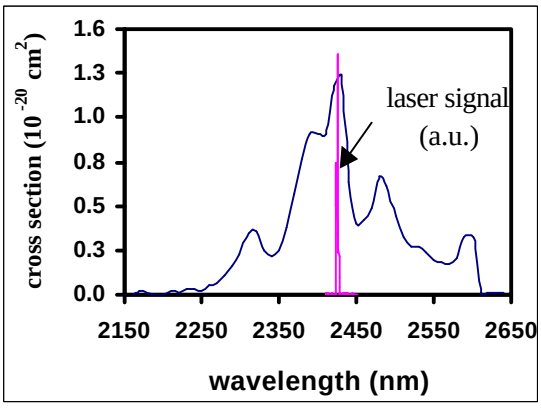

Figure 6. Emission spectrum and laser output near 2.4 μm in $CaGa_2S_4:Dy^{3+}$.

$CaGa_2S_4:Dy^{3+}$ 4.31 μm laser results

Four cavity mirrors were employed for 4.3 μm operation with transmissions of 0.84% (HR), 0.84%, 2.55%, and 5.25%. Data was recorded for three mirror configurations with total transmissions (high reflector + output coupler) of 1.68%, 3.39%, and 6.09%. Due to strong fundamental CO_2 absorption, the cavity was purged with dry nitrogen for operation near 4.3 μm. Slope efficiency curves are shown in Figure 7 for two of these configurations, and all data are summarized in Table 3. Predictions again agreed relatively well with the measured thresholds, but were an order of magnitude higher than the measured slope efficiencies. A Findlay-Clay plot of transmission vs. threshold energy is shown in Figure 8, yielding a passive loss of L = 0.9% +/- 0.3%. The lower loss at 4.31 μm vs. 2.43 μm is perhaps expected if the scattering losses obey a Rayleigh λ^{-4} dependence. Notice that the slope efficiencies do not vary greatly with the different output coupler reflectivities. This is expected since the passive losses are small compared to the output coupling in each case, although there appears to be additional losses not compensated by greater output coupling (such as optical aberrations in the sample). AR-coated samples, planned for future experiments, may perform better.

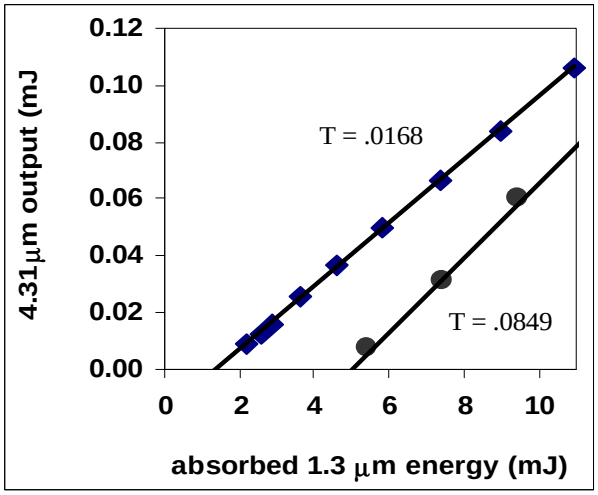

Figure 7. Slope efficiency curves for $CaGa_2S_4:Dy^{3+}$ at 4.31 μm.

Table 3. Summary of $CaGa_2S_4:Dy^{3+}$ 4.31 μm laser results.

Total output coupling (%)	Threshold (mJ)	Slope efficiency (%)
1.7	1.3	1.1
3.4	2.4	1.6
8.5	5.2	1.4

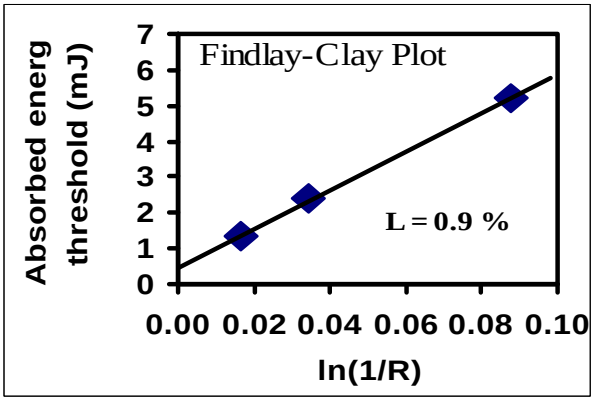

Figure 8. Plot of absorbed energy threshold vs. total transmission.

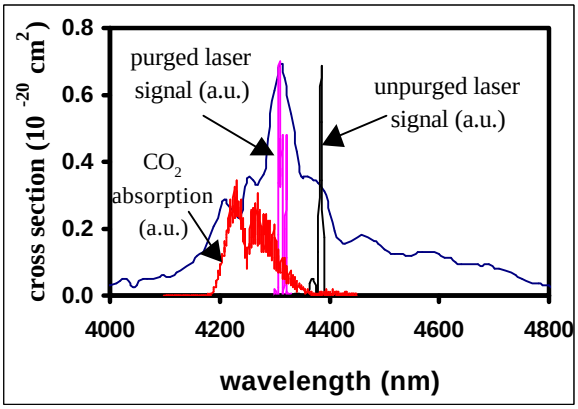

Figure 9. Emission spectrum and laser output near 4.3 μm in $CaGa_2S_4:Dy^{3+}$. The longer wavelength signal results from an unpurged cavity. When purged

with nitrogen, the laser operates at the peak of the fluorescence spectrum.

The laser output and fluorescence emission spectrum is shown in Figure 9. The laser output of an unpurged cavity (peak wavelength 4.38 μm) is also shown in this figure for comparison. The extra loss imposed by the CO_2 absorption forced the laser to operate at a longer wavelength. The purged-cavity laser spectrum near 4.31 μm includes the CO_2 absorption along the ~2 meters of unpurged pathlength between the laser and the monochromator. The laser light was determined to be polarized along the 'fast' axis, similar to the 2.43 μm laser output. These data can be compared with the results given in Ref. 6 for the Dy^{3+}:YLF laser operating at 4.34 μm, where a 1.7 μm, 150 ns pump pulse was employed to directly populate the upper $^6H_{11/2}$ laser level. Although the cavity geometries, crystal properties, pumping schemes, etc. are different, and the low $CaGa_2S_4:Dy^{3+}$ slope efficiencies not withstanding, the performance of these two lasers is roughly commensurate. A comparison of the $CaGa_2S_4:Dy^{3+}$ and Dy^{3+}:YLF lasers is given in Table 4.

Table 4. Comparison of $CaGa_2S_4:Dy^{3+}$ and Dy^{3+}:YLF lasers operating near 4.3 μm

Host	**λ_{pump} (μm)**	**λ_{laser} (μm)**	**τ_{upper} (μs)**	**η (%)**	**Minimum threshold* (mJ)**	**Maximum slope efficiency* (%)**
$CaGa_2S_4$	1.3	4.31	3020	73	1	1.6
YLF	1.7	4.34	0.8	<0.01	10	5.2

* experimentally measured

KPb_2Cl_5 physical properties/crystal growth

Crystals of dysprosium doped KPb_2Cl_5 were grown at the Design and Technical Institute of Monocrystals by the Bridgman technique. KPb_2Cl_5 is biaxial and belongs to the monoclinic crystal class.[8] Dy^{3+} was doped on the Pb^{2+} site to a measured concentration of 3.5×10^{19} cm^{-3} (0.75 mol% in the melt and a 100% distribution coefficient). K^+ vacancies are assumed to provide charge compensation[9]. The 6.4 mm sample was oriented with a polariscope so that the optic axis was nearly parallel to the acute bisectrix of the biaxial indicatrix. The two optic axes were not resolvable with the unaided eye under the polariscope, implying a low birefringence in this material.

$KPb_2Cl_5:Dy^{3+}$ spectroscopy

In our previous work,[1] spectroscopic data such as absorption cross sections, emission cross sections (σ_{em}), and lifetimes (τ_{upper}) were measured for a sample of $KPb_2Cl_5:Dy^{3+}$. This data was used to perform a Judd-Ofelt analysis, giving rise to spectroscopic data such as radiative lifetimes (τ_{rad}), branching ratios (β), and radiative quantum yields ($\eta = \tau_{upper}/\tau_{rad}$). Table 5 gives a summary of the relevant data for this laser crystal. Figure 10 shows the unpolarized absorption spectrum. The hypersensitive nature of the 1.3 μm absorption feature in this material might undermine the accuracy of the Judd-Ofelt model for $KPb_2Cl_5:Dy^{3+}$, as evidenced by the high 2.4 μm radiative quantum yield in Table 5.

$KPb_2Cl_5:Dy^{3+}$ Experimental setup

The laser setup used for $KPb_2Cl_5:Dy^{3+}$ is identical to that used for $CaGa_2S_4:Dy^{3+}$. In this case, however, no distinction is made between the 'slow' and 'fast' crystallographic axes since they are nearly identical in this sample. The input beam was kept at a single polarization for convenience. A wedge angle of ~2 mrad was determined by examination of reflections of a single He-Ne laser beam from both end faces of the laser polished sample.

Table 5. Spectroscopic data for $KPb_2Cl_5:Dy^{3+}$.

Transition	λ (μm)	τ_{upper} (ms)	τ_{rad} (ms)	η (%)	β (%)	σ_{em} (10^{-20} cm^2)
$^6H_{9/2}$-$^6F_{11/2}$ → $^6H_{13/2}$	2.4	0.58	0.55	100	5	0.8
$^6H_{11/2}$ → $^6H_{13/2}$	4.3	6.94	8.86	78	13	0.6

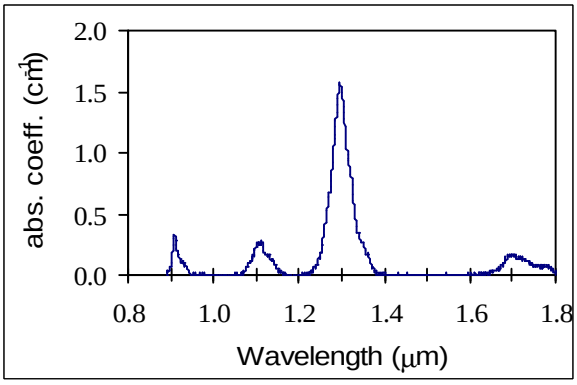

Figure 10. Unpolarized emission spectrum for $KPb_2Cl_5:Dy^{3+}$.

$KPb_2Cl_5:Dy^{3+}$ 2.43 μm laser results

Data was recorded for three mirror configurations with total transmissions of 0.94%, 2.23%, and 8.28%. The high reflector in each case had a transmission of 0.58%. Slope efficiency curves are shown in Figure 11 for two of these configurations, and all are summarized in Table 6. Again, predictions agreed relatively well with the measured thresholds, but were an order of magnitude higher than the measured slope efficiencies. A Findlay-Clay plot of absorbed energy threshold vs. transmission is shown in Figure 12, yielding a round-trip passive loss of L = 1.2% +/- 0.4%. The laser output spectrum is shown in Figure 13, along with the unpolarized emission spectrum, showing that laser action occurs at the fluorescence peak. The laser light was determined to be unpolarized as expected due to the orientation of the crystal near the optic axis.

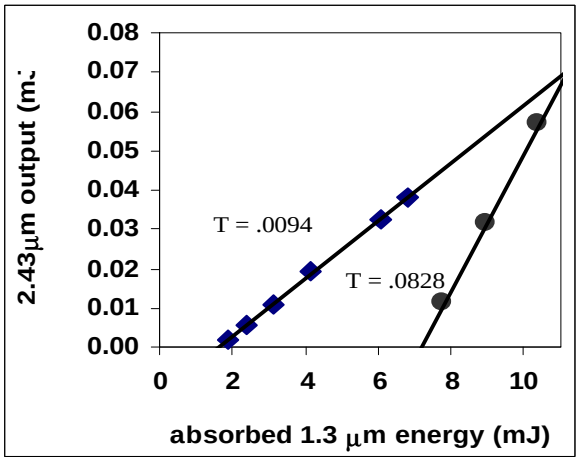

Table 6. Summary of $KPb_2Cl_5:Dy^{3+}$ 2.43 μm laser results

Total output coupling (%)	Threshold (mJ)	Slope efficiency (%)
0.9	1.6	0.7
2.2	2.5	2.2
8.3	7.2	1.7

Figure 11. Slope efficiency curves for $KPb_2Cl_5:Dy^{3+}$ at 2.43 μm.

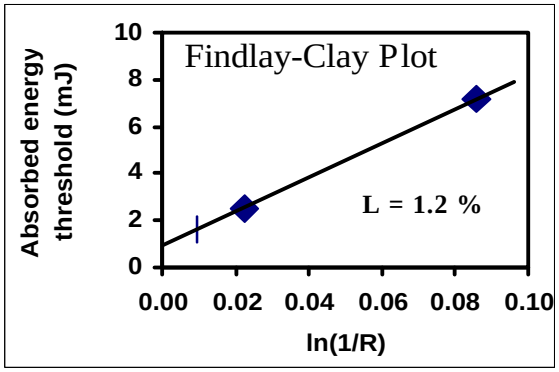

Figure 12. Plot of absorbed energy threshold vs. total transmission

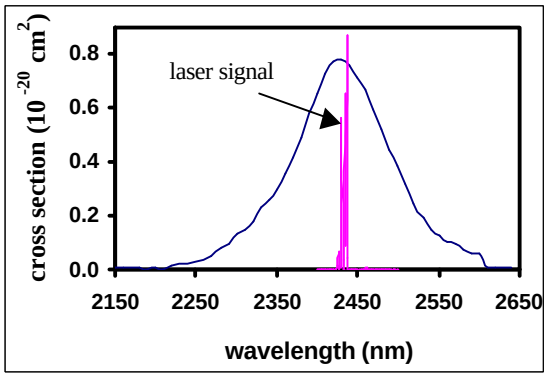

Figure 13. Emission spectrum and laser output near 2.4 μm in $KPb_2Cl_5:Dy^{3+}$.

Discussion

We have demonstrated mid-infrared laser action for the KPb_2Cl_5 and $CaGa_2S_4$ laser hosts for the first time. These materials possess high radiative quantum efficiency. The superior radiative quantum efficiency of KPb_2Cl_5 and $CaGa_2S_4$ is summarized in Table 7, where we have included Dy^{3+}:GaLaS [10] glass in the comparison of the $^6H_{11/2} \rightarrow {}^6H_{13/2}$ Dy^{3+} transition with these hosts. The measurement of thermo-mechanical properties for KPb_2Cl_5 and $CaGa_2S_4$ will be the subject of future experiments.

Table 7. Radiative quantum efficiency comparison for the 4.3 μm Dy^{3+} transition in various hosts.

Dy^{3+} Host	λ (μm)	τ_{upper} (ms)	τ_{rad} (ms)	η
KPb_2Cl_5	4.25	6.94	8.86	78%
$CaGa_2S_4$	4.31	3.02	4.16	73%
GaLaS glass[10]	4.27	3.60	6.29	57%
YLF[6]	4.34	0.8×10^{-3}	~18	< 0.01%

Conclusions

$CaGa_2S_4$ (calcium thiogallate) and KPb_2Cl_5 (potassium lead chloride) have proven to be viable, non-hygroscopic host materials for mid-IR lasing. We have demonstrated room temperature laser action at 2.43 and 4.31 μm in $CaGa_2S_4:Dy^{3+}$ and at 2.43 μm in $KPb_2Cl_5:Dy^{3+}$. Future experiments involving direct pumping of the $^6H_{11/2}$ upper laser level at 1.7 μm should permit 4.3 μm lasing in $KPb_2Cl_5:Dy^{3+}$ and improved slope efficiency at 4.3 μm for $CaGa_2S_4:Dy^{3+}$.

A special thanks is extended to Peter Thelin for his efforts in the polishing of the laser crystals. This work was supported by DARPA and BES, and we are grateful to L.N. Durvasula for his interest in this work.

LLNL personnel performed this work under the auspices of the U.S. Department of Energy, Lawrence Livermore National Laboratory, Contract No. W-7405-ENG-48.

References

[1] M.C. Nostrand, R.H. Page, S.A. Payne, W.F. Krupke, and P.G. Schunemann, *ASSL TOPS* **XIX,** 524 (1998)
[2] P.N. Kumta and S.H. Risbud, *J. Mater. Sci*. **29**, 1135 (1994)
[3] T.E. Peters and J.A. Baglio, *J. Electrochem. Soc.* **119**, 230 (1972)
[4] R. Ibanez, A. Garcia, C. Fouassier, and P. Hagenmuller, *J. Solid State Chem* **53**, 406 (1984)
[5] J.A. Caird, S.A. Payne, P.R. Staver, A.J. Ramponi, LL. Chase and W.F. Krupke, *IEEE J. Quantum Electron.* **24**, 1077 (1988)
[6] N.P. Barnes and R.E Allen, *IEEE J. Quantum Electron.* **27**, 277 (1991)
[7] W. Koechner, *Solid-State Laser Engineering.* New York:Springer, 1996
[8] K. Nitsch, M. Dusek, M. Nikl, K. Polak and M. Rodova, *Prog. Crystal Growth and Charact.* **30**, 1 (1995)
[9] L.I Isaenko, *Photonics West* (SPIE, San Jose, 1998), paper 3265-31
[10] T. Schweizer, D.W. Hewak, B.N. Samson, and D.N. Payne, *Optics Letters* **21**, 1594 (1996)